

See discussions, stats, and author profiles for this publication at: <https://www.researchgate.net/publication/258837113>

Influence of Incorporating Different Electron-Rich Thiophene-Based Units on the Photovoltaic Properties of Isoindigo-Based Conjugated Polymers: An Experimental and DFT Study

ARTICLE *in* MACROMOLECULES · NOVEMBER 2013

Impact Factor: 5.8 · DOI: 10.1021/ma401691r

CITATIONS

27

READS

25

11 AUTHORS, INCLUDING:



Patrik Henriksson

Chalmers University of Technology

20 PUBLICATIONS 599 CITATIONS

[SEE PROFILE](#)



Renee Kroon

Chalmers University of Technology

21 PUBLICATIONS 665 CITATIONS

[SEE PROFILE](#)



Ergang Wang

Chalmers University of Technology

71 PUBLICATIONS 2,443 CITATIONS

[SEE PROFILE](#)



Mats R. Andersson

Chalmers University of Technology

196 PUBLICATIONS 8,354 CITATIONS

[SEE PROFILE](#)

Influence of Incorporating Different Electron-Rich Thiophene-Based Units on the Photovoltaic Properties of Isoindigo-Based Conjugated Polymers: An Experimental and DFT Study

Wenliu Zhuang,^{*,†} Margherita Bolognesi,[‡] Mirko Seri,[§] Patrik Henriksson,[†] Desta Gedefaw,[†] Renee Kroon,[†] Markus Jarvid,[†] Angelica Lundin,[†] Ergang Wang,[†] Michele Muccini,^{||} and Mats R. Andersson^{*,†}

[†]Department of Chemical and Biological Engineering, Polymer Technology, Chalmers University of Technology, SE-412 96 Göteborg, Sweden

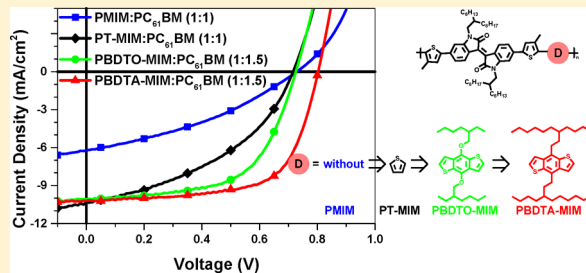
[‡]Laboratory MIST E-R, Via P Gobetti 101, 40129 Bologna, Italy

[§]Istituto per la Sintesi Organica e la Fotoreattività (ISOF), Consiglio Nazionale delle Ricerche (CNR), Via P. Gobetti 101, 40129 Bologna, Italy

^{||}Istituto per lo Studio dei Materiali Nanostrutturati (ISMN), Consiglio Nazionale delle Ricerche (CNR), Via P. Gobetti 101, 40129 Bologna, Italy

Supporting Information

ABSTRACT: A series of novel donor–acceptor conjugated alternating copolymers based on the isoindigo acceptor moiety have been designed, synthesized, and characterized, in order to explore the potential of isoindigo for efficient donor materials with high photovoltages in solar cells. We have systematically investigated and discussed the effect of combining different electron-rich thiophene-based units on the structural, optical, electronic, and photovoltaic properties of the resulting polymers. Morphological studies and quantum-chemical calculations are carried out to gain insights into the different properties. The power conversion efficiencies (PCEs) of the solar cells based on these polymers are increased step by step through a rational structural modification. Among them, PBDTA-MIM shows a PCE of 5.4%, which is to our knowledge the best result achieved among isoindigo-based polymers for solar cells combined with PC₆₁BM as the acceptor using the conventional device configuration. Our results further emphasize the use of isoindigo as an effective acceptor unit and highlight the importance of carefully choosing appropriate chemical structure to design efficient donor–acceptor polymers for organic solar cells. In addition, the resulting low optical gaps, the promising PCEs with PC₆₁BM as the acceptor, and the good open-circuit voltages (up to 0.8 V) synergistically demonstrate the potential of this class of polymers as donor materials for bottom subcells in organic tandem solar cells.



INTRODUCTION

Polymer solar cells (PSCs) are a promising technology for producing clean and renewable energy, based on solution-processed, lightweight, potentially flexible devices.¹ The current challenges for PSCs are to improve photovoltaic efficiency, cost-effectiveness, and durability. The state-of-the-art device architectures of PSCs to date are based on the concept of a bulk heterojunction (BHJ)² as the active layer, which typically consists of a bicontinuous interpenetrating blend of an electron-donating polymer and an electron-accepting fullerene derivative. The power conversion efficiency (PCE) of PSCs during the past 4 years has improved rapidly from 5% to approximately 10%,^{1a,3} mainly due to the design and synthesis of new electron-donating conjugated polymers with desirable chemical and physical properties (i.e., to control frontier molecular orbital energies and molecular ordering) and

optimization of device fabrication (i.e., to control active layer morphology and interfacial engineering).^{1a,4}

An efficient method to obtain conjugated polymers is based on the strategy of donor–acceptor polymers,⁵ by combining π -electron-rich (donor) and π -electron-deficient (acceptor) conjugated moieties into their repeating units. This particular method allows control of the band gap and energy levels of conjugated polymers by choosing appropriate donor and acceptor moieties, with the donor typically determining the energy level of the highest occupied molecular orbital (HOMO) and the acceptor, the lowest unoccupied molecular orbital (LUMO).⁶ To push the efficiency toward the theoretical

Received: August 12, 2013

Revised: September 29, 2013

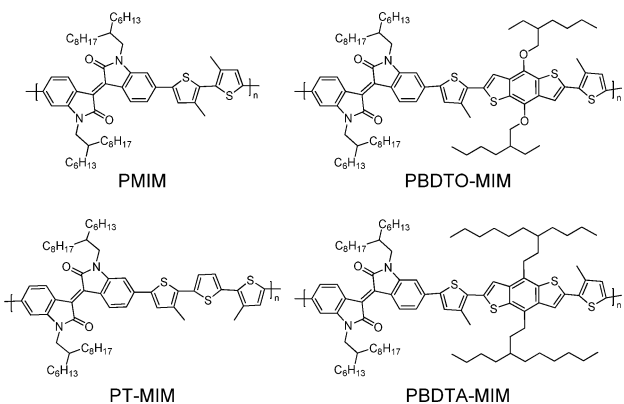
Published: October 16, 2013

limit in single-junction photovoltaic cells, achieving both a high short-circuit current density (J_{SC}) and a high open-circuit voltage (V_{OC}) is crucial, along with a high fill factor (FF). Both J_{SC} and V_{OC} are influenced by the band gap of the photoactive material and by the alignment of the HOMO and LUMO energy levels with respect to those of the acceptor material used in the active blend. Note that the PCE is not monotonically correlated to either the band gap of the donor material or the LUMO-level offset of the donor to the acceptor, but both of them need to be optimized independently, from a materials chemist's point of view.^{6b,7}

In the exploration of new electron-donating materials, semiconductors based on isoindigo—possessing a ketopyrrole-containing core of two lactam rings with a strong electron affinity—have attracted increasing attention due to their potential in optoelectronic devices.⁸ Although being already known for over a century,⁹ isoindigo was first introduced only in 2010 by Reynolds and co-workers as an effective building unit for new conjugated molecular materials and polymers.^{8a,b} Our recent studies demonstrated the potential of isoindigo as an efficient acceptor unit in donor–acceptor polymers for BHJ solar cells.^{8d,i,j,l} Among these, PTI-1, consisting of alternating thiophene and isoindigo units, with an optical gap of 1.6 eV, shows a PCE of 3.0% with a V_{OC} of 0.89 V, J_{SC} of 5.4 mA/cm², and FF of 63% when combined with PC₇₁BM ([6,6]-phenyl-C₇₁-butyric acid methyl ester) as the acceptor in BHJ devices.^{8d} Extending the conjugation length of the donor unit in PTI-1 from thiophene to a terthiophene derivative resulted in a more efficient donor polymer, P3TI, with a reduced optical gap (1.5 eV). P3TI shows a PCE of 6.3% in the same device configuration, with a V_{OC} , J_{SC} , and FF of 0.70 V, 13.1 mA/cm², and 69%, respectively.⁸ⁱ Notably, even though a high PCE was achieved for P3TI, the V_{OC} was not prominent, while for PTI-1, even though a V_{OC} up to 0.9 V was obtained, the PCE was moderate. The initial success of isoindigo-based polymers for organic solar cells^{8c–e,i,j,l,10} motivated us to further explore the possibility of improving the photovoltaic performance in these systems, especially by combining a high PCE and a high V_{OC} into one single isoindigo-based polymer, as well as to investigate their structure–property relationships.

In this work we report on the synthesis, characterization, and structure–property relationships of a series of novel electron donor polymers (PMIM, PT-MIM, PBDTO-MIM, and PBDTA-MIM, Chart 1), which combine the same isoindigo acceptor moiety with different thiophene-based donor units.

Chart 1. Chemical Structures of PMIM, PT-MIM, PBDTO-MIM, and PBDTA-MIM

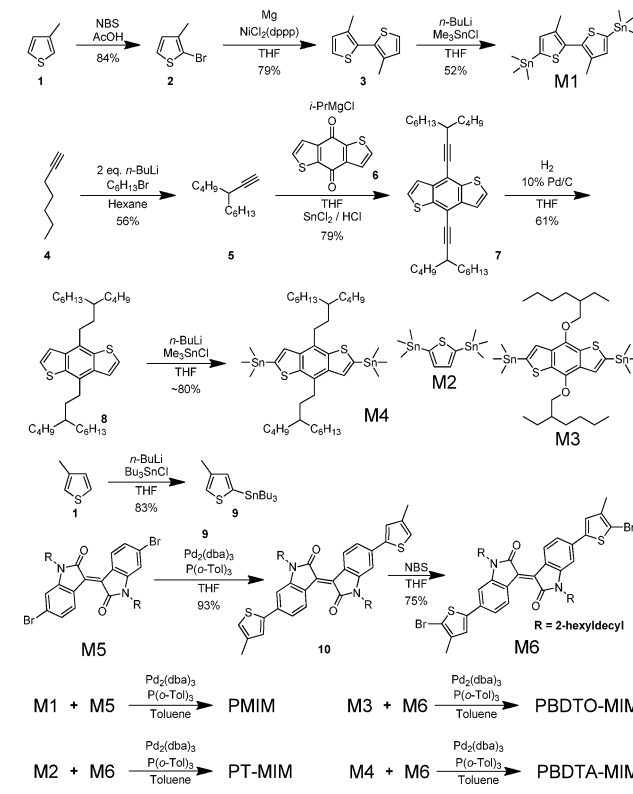


We systematically investigate the effect of these different electron-rich units on the chemical, optical, electronic, morphological, and photovoltaic properties of the resulting isoindigo-based conjugated polymers. We find that the PCEs of the resulting PSCs can be improved by over 3-fold through a rational structural modification of the donor moiety. Among the four resulting isoindigo-based polymers, PBDTA-MIM in combination with PC₆₁BM ([6,6]-phenyl-C₆₁-butyric acid methyl ester) shows a PCE of 5.4%, which is to the best of our knowledge the highest value for conventional BHJ solar cells with isoindigo-based polymers blended with PC₆₁BM. Considering the relatively low optical gaps (1.5–1.7 eV) of these polymers, the promising PCE of PC₆₁BM-based devices along with their resulting good V_{OC} (at least 0.8 V) synergistically makes this class of polymers suitable candidates as donor components for the bottom active layer in tandem solar cells.^{7b}

RESULTS AND DISCUSSION

Material Design, Synthesis, and Structural Characterization. Four donor–acceptor alternating copolymers (Chart 1) were synthesized according to Scheme 1. Previous work on

Scheme 1. Synthesis of Monomers and Polymers



isoindigo polymers has shown that extending the conjugation in the donor moieties from a single thiophene (PTI-1)^{8d} to terthiophene (P3TI)⁸ⁱ resulted in a decreased V_{OC} by ~0.2 V, even though the PCE was more than doubled. In this study, the bithiophene unit was employed to have an intermediate π -conjugation length in the donor moiety, resulting in donor–acceptor polymer PMIM. The introduction of methyl groups on the bithiophene unit would be expected to give a slightly twisted backbone, which should increase the band gap and thus the V_{OC} .¹¹ Meanwhile, a beneficial intermolecular stacking

might still occur by adopting conformations where the two methyl substituents on the adjacent thiophene units are away from each other,¹² favoring a linear backbone in the solid state.¹³ For comparison, a thiophene ring was inserted in between the two alkylthiophene units to have the same polymer backbone as P3TI (the best-performing isoindigo-based polymer reported so far),⁸ⁱ resulting in PT-MIM. To further extend the π -conjugation length of the donor unit, benzo[1,2-*b*:4,5-*b'*]dithiophene (BDT) was also incorporated. Recently, BDT has been widely used as an effective electron-rich building block thanks to its desirable properties such as structural rigidity, planarity, and favorable interchain π - π stacking, along with the presence of additional substitution sites for the incorporation of side chains.^{4a-h,k,p} Here the BDT unit with two 2-ethylhexyloxy side chains was used to replace the middle thiophene in the terthiophene unit in PT-MIM, resulting in PBDTO-MIM. Notably, similar polymers with identical backbones (PBDT-TIT and PBDT-OIO) showed promising device performance with a V_{OC} up to 0.79 V, J_{SC} of 7.87 mA/cm², FF of 68%, and a PCE of 4.22%.⁸ⁱ Furthermore, it is known that removal of oxygen from the side chains of the donor unit can reduce the electron density, to allow for a deeper HOMO energy level, which in principle should enhance the V_{OC} of the resulting PSCs.¹⁴ Hence, the alkoxy side chains on the BDT unit were replaced with branched alkyl chains, resulting in PBDTA-MIM.

The synthesis of the monomers is outlined in Scheme 1. Monomer 5,5'-bis(trimethylstannyl)-3,3'-dimethyl-2,2'-bithiophene (**M1**) was readily prepared through a three-step procedure starting from commercially available 3-methylthiophene (**1**). First, bromination of **1** with *N*-bromosuccinimide (NBS) in acetic acid gave 2-bromo-3-methylthiophene (**2**) in 82% yield, which was followed by a nickel-catalyzed Kumada coupling to afford 3,3'-dimethyl-2,2'-bithiophene (**3**) in 79% yield. Finally, lithiation with *n*-butyllithium and stannylation with trimethyltin chloride resulted in monomer **M1** in reasonable yield. Monomer 2,6-bis(trimethylstannyl)-4,8-bis(3-butynonyl)benzo[1,2-*b*:4,5-*b'*]dithiophene (**M4**)^{4e,f} was prepared according to modified literature procedures.^{14b,15} Monomer 6,6'-bis(5-bromo-4-methylthiophen-2-yl)-*N,N'*-bis(2-hexyldecyl)isoindigo (**M6**) was prepared from *N,N'*-bis(2-hexyldecyl)-6,6'-dibromoisoindigo (**M5**) following the procedure described in our previous work,^{8d,i} except tributyl(4-methylthiophen-2-yl)stannane (**9**)¹⁶ was used instead of tributyl(4-octylthiophen-2-yl)stannane. Compound **9** was prepared from 3-methylthiophene (**1**) by lithiation with *n*-butyllithium at -78 °C and stannylation with tributyltin chloride in quantitative conversion but with a regioselectivity¹⁷ of 4:1 over the isomer tributyl(3-methylthiophen-2-yl)stannane as determined by ¹H NMR. The use of this product without further purification in the Stille coupling with dibromide **M5** turned out to give a satisfactory selectivity, which is probably due to the use of compound **9** in large excess as well as its inferior steric hindrance effect in comparison with the unwanted regioisomer in the reaction. *N,N'*-Bis(2-hexyldecyl)-6,6'-bis(4-methylthiophen-2-yl)isoindigo (**10**) was obtained in above 90% yield based on compound **M5**, and subsequent bromination with NBS in THF afforded monomer **M6** in 75% yield after column chromatography and recrystallization.

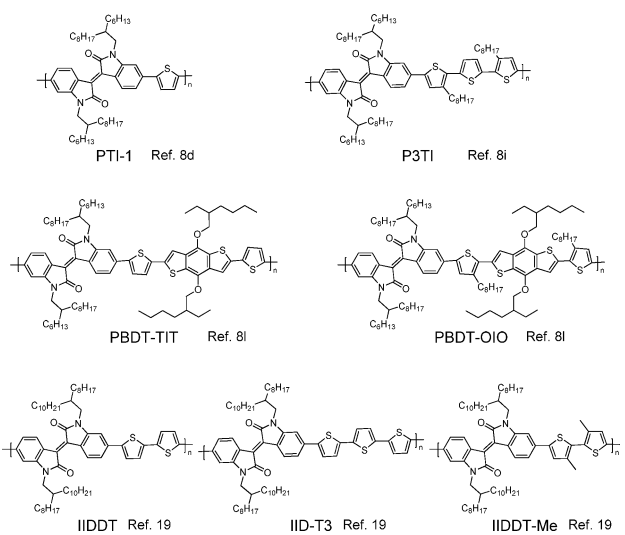
All the polymers were synthesized via Stille coupling reaction¹⁸ from the corresponding monomers as shown in Scheme 1. After the reaction mixture was precipitated into methanol, the polymers were collected and washed via Soxhlet

extraction with methanol, acetone, ether, hexane, dichloromethane, and chloroform successively. The chloroform fraction was precipitated into methanol, and the final products were collected by filtration and dried under vacuum. The molar masses of the four polymers were determined by size-exclusion chromatography (SEC) relative to uniform polystyrene. The corresponding number-average degrees of polymerization (X_n) were also calculated for comparison. In order to obtain high relative molecular masses, the equimolar feed ratios of the respective monomers and the polymerization time were carefully controlled until precipitation of the resulting polymers began to occur.

PMIM had a number-average molar mass (M_n) of 20.1 kDa with a molar-mass dispersity (D_M) of 2.1 ($X_n = 22.3$). It should be mentioned that a hot chlorobenzene fraction after chloroform extraction gave a comparable yield of PMIM, with a much higher M_n of 62.8 kDa ($D_M = 1.9$, $X_n = 69.7$), which is not considered for comparison in this work because it was not processable from common organic solvents at the concentrations needed for devices preparation (see also further discussions about absorption in solution). Note that the polymerization of PMIM was very fast (15 min at 95 °C). Therefore, for the other three polymers lower concentrations were employed to obtain good amounts of soluble polymers from hot chloroform fraction. Going from PMIM to PT-MIM resulted in a slightly lower M_n of 13.4 kDa for PT-MIM ($D_M = 1.8$, $X_n = 13.6$), indicating a decreased solubility. Note that both PMIM and PT-MIM had a lower X_n (and M_n) than their respective analogues IIDDT and IID-T3 (without any substituent on the thiophene rings but with slightly longer side chains on the isoindigo) from the chloroform-soluble fractions (IIDDT: $M_n = 33.7$ kDa, $D_M = 5.4$, $X_n = 34.2$; IID-T3: $M_n = 33.8$ kDa, $D_M = 3.4$, $X_n = 36.3$).¹⁹ Given their same backbone structures, the solubility can vary because of the difference in the side chains on the isoindigo units (2-hexyldecyl in this work and 2-octyldecyl in the literature) as well as on the flanking thiophenes (with or without methyl groups, respectively). In fact, the introduction of methyl groups on the flanking thiophenes did not guarantee increased molar masses for the resulting polymers with sufficient solubility, for example, going from IIDDT to IIDDT-Me ($M_n = 20.1$ kDa, $D_M = 3.9$, $X_n = 17.2$) in the same literature,¹⁹ probably due to an increased rotational barrier between adjacent thiophene rings (with head-to-head linkages in the presence of substituents).¹² Also, different polymerization conditions can further explain the observed variation of the relative molecular masses. By replacing the unsubstituted thiophene with a BDT unit with alkoxy or alkyl branched side chains, a dramatic improvement in terms of solubility and molar masses of the polymers occurred (PBDTO-MIM: $M_n = 63.5$ kDa, $D_M = 3.0$, $X_n = 47.2$; PBDTA-MIM: $M_n = 69.3$ kDa, $D_M = 4.0$, $X_n = 47.7$).²⁰ Finally, all the polymers in this study were washed with the same solvents by Soxhlet extraction as mentioned before, obtained from the chloroform fraction, and were soluble in common solvents such as chloroform, chlorobenzene, *o*-dichlorobenzene (DCB), etc. The comparison of these polymers in this work is therefore more based on a compromise between sufficient solubility and high molar masses, both of which are relevant properties to the solution-processing conditions and film morphology.²¹

Optical and Electrochemical Properties. The normalized UV-vis absorption spectra both in DCB solution and in pristine films of the four polymers are shown in Figure 1. We

Chart 2. Chemical Structures of Some Isoindigo-Based Polymers in the Literature



first considered the optical properties from film absorption (Figure 1A). All of these polymers show dominant absorption bands in the long-wavelength side (around 600–660 nm), which can be assigned to the intramolecular HOMO → LUMO transitions from the ground state (S_0) to the excited state (S_1).²² The appearance of extra peaks or vibrational shoulders in the long-wavelength side (ca. 670–750 nm) of the absorption spectra for all of these polymers might originate from intermolecular transitions.²³ According to the absorption spectra of the films (Figure 1A), the optical gaps of the polymers, deduced from their absorption edges, are 1.53 eV for PMIM, 1.57 eV for PT-MIM, and 1.66 eV for PBDTO-MIM and PBDTA-MIM (Figure 2).

In the solid state, the optical gap of PMIM is slightly lower than that of the analogous IIDDT ($E_g = 1.59$ eV), even though PMIM has a shorter polymer chain than IIDDT as can be seen from their X_n 's (22.3 vs 34.2).¹⁹ This indicates that PMIM has a better conjugation pathway, probably due to a favored conformation with the two methyl groups on the bithiophene unit away from each other, along with an increased inter-ring rotational barrier, favoring a linear polymer backbone and an improved interchain packing in the solid state.^{12,13} PMIM can absorb light up to ca. 810 nm in the solid state, which would be beneficial for achieving high photocurrents. Going from PMIM to PT-MIM resulted in an unexpected blue-shift of ca. 20 nm in the solid state, while the insertion of thiophene unit should have decreased the band gap for PT-MIM as compared with PMIM. This is probably due to increased backbone flexibility in the absence of head-to-head linkages in the donor moiety as

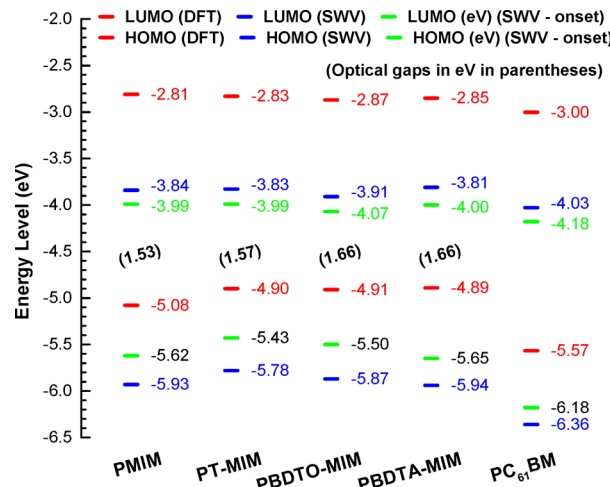


Figure 2. Energy levels estimated from DFT at the B3LYP/6-31G(d) level and from SWV and optical gaps from film absorption.

well as the reduction in polymer chain length suffering from the decreased solubilizing side chain density. In contrast, the analogous P3TI, with long alkyl side chains on the flanking thiophenes (i.e., octyl vs methyl),⁸ⁱ shows a smaller optical gap (1.50 eV for P3TI vs 1.57 eV for PT-MIM), presumably because P3TI has a polymer chain ca. 3 times as long as PT-MIM, as implied by the obtained molar masses (M_n over 43 kDa for P3TI and only 13 kDa for PT-MIM) and degrees of polymerization (X_n of 36.4 for P3TI vs 13.6 for PT-MIM). This corresponds to a difference of around 38 nm in their optical gaps and indicates PT-MIM may have a conjugation path length shorter than its effective conjugation length. Further comparison with another analogue IID-T3 ($E_g = 1.58$ eV, $X_n = 36.3$)¹⁹ implies that PT-MIM ($E_g = 1.57$ eV, $X_n = 13.6$) has a better conjugation pathway to narrow the band gap than IIDT-3, which may benefit from the introduction of methyl groups on the flanking thiophenes, favoring a good interchain packing or a linear backbone in the solid state.¹³ These comparisons can explain the observed blue-shift going from PMIM to PT-MIM. Insertion of BDT units instead of thiophene in the polymer backbone gave an even larger blue-shift in the solid state (up to around 60 nm) as compared with PMIM, regardless of alkoxy (PBDTO-MIM) or alkyl (PBDTA-MIM) side chains attached. PBDTO-MIM and PBDTA-MIM have a very similar X_n of around 47 and optical gap (only 3 nm blue-shifted from PBDTO-MIM to PBDTA-MIM), indicating that the two polymers have similar effective conjugation lengths.

We also compared the UV-vis absorption of the four polymers in DCB solution (Figure 1B). The solutions were prepared in a concentration dilute enough so that the as-

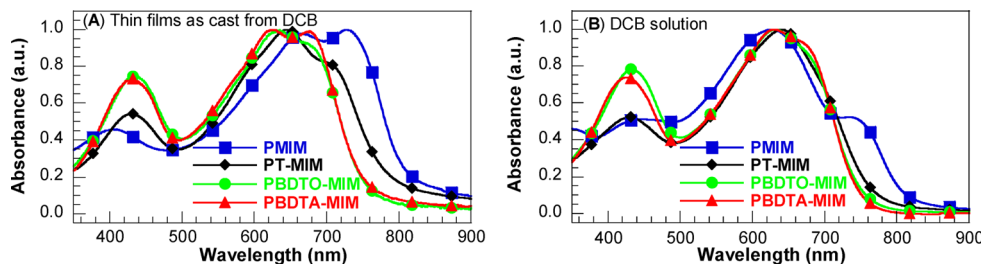


Figure 1. UV-vis absorption spectra of the four isoindigo-based polymers (A) in the solid state and (B) in DCB solution.

recorded absorbance maxima at the low-energy side approached unity (corresponding to nearly 90% absorption of the incident light at most). For PMIM and PT-MIM, the absorption spectra show a red-shift going from solution to films, indicating that there are aggregations and/or orderly π - π stacking formed in the solid state. For PMIM we did not observe an obvious blue-shifted absorption from film to solution, which was reported for the aforementioned IIDDT-Me.¹⁹ Instead we observed, even in the dilute solution, a lower energy shoulder, the relative intensity of which could be decreased with heating, but did not vanish with further heating (Figure S1, Supporting Information), indicating a strong aggregation tendency for PMIM. The difference between PMIM and IIDDT-Me may be due to the fact that longer branched side chains were employed, but shorter polymer main chains were obtained for IIDDT-Me, resulting in a higher solubility, than for PMIM (see above). The strong aggregation tendency of PMIM can also be accountable for the exclusion in this study of the aforementioned much higher molar mass fraction suffering from poor solubility and poor film-forming ability. However, for the two BDT-based polymers, only a slight difference has been observed between the absorption spectra in solution and in thin films, probably indicating a more rigid planar conformation, which is a typical phenomenon in the reported isoindigo-based polymers.^{8b,c,19,24} It has been shown that there is no obvious aggregation in solution or in thin films for polymers based on PBDTO-MIM analogues with either much longer side chains (PBDT-OIO) or no substituents (PBDT-TIT) on the thiophene spacer due to the bulky branched side chains on the acceptor units.⁸ⁱ Considering the chemical structure and the above-obtained molar masses for PBDTO-MIM and PBDTA-MIM, these two BDT-based polymers should show absorption coefficients comparable to PBDT-OIO and PBDT-TIT.⁸ⁱ

The HOMO and LUMO energy levels of the polymers (Figure 2, blue lines) were deduced from their respective ionization potentials and electron affinities estimated by square-wave voltammetry (SWV) (Figure S2, Supporting Information) from the first oxidation and reduction peak potentials, respectively. All the polymers exhibit deeply low-lying HOMO levels, in the order: PBDTA-MIM (-5.94 eV) < PMIM (-5.93 eV) < PBDTO-MIM (-5.87 eV) < PT-MIM (-5.78 eV).^{6b} Going from PMIM to PT-MIM slightly raised the HOMO level, and thereby gave a lower offset to the LUMO energy level of PCBM, which is regarded to be the maximum value for V_{OC} .^{6b,8i} It is noteworthy that this was accompanied by a slightly larger optical gap for PT-MIM as discussed above. On the other hand, the incorporation of BDT units resulted in relatively deeper HOMO energy levels (-5.87 eV for PBDTO-MIM and -5.94 eV for PBDTA-MIM) than that of PT-MIM (-5.78 eV) (and P3TI), comparable to that of PMIM (-5.93 eV). Note that by replacing the alkoxy side chains with the less electron-donating alkyl chains (going from PBDTO-MIM to PBDTA-MIM), the HOMO energy level was lowered by 0.07 eV, which would be expected to result in a higher V_{OC} for PSCs based on PBDTA-MIM than that for PBDTO-MIM.

The LUMO levels of the polymers are very low-lying, which can be ascribed to their same isoindigo units. This is because the LUMO levels of donor–acceptor polymers are mainly governed by the electron-deficient units,^{6b,e} and unlike the HOMO levels, the LUMO levels are less affected by the conjugation length of the polymers. Given that the contribution of the isoindigo moiety to the LUMO level should be similar,

the variation in the LUMO energy level therefore mainly depends on the nature of the donor units. The estimated LUMO energy levels of the four polymers follow the order PBDTO-MIM (-3.91 eV) < PMIM (-3.84 eV) < PT-MIM (-3.83 eV) < PBDTA-MIM (-3.81 eV). For comparison, energy levels deduced from the first reduction and oxidation peak potentials of $PC_{61}BM$ are also included in Figure 2. The LUMO-level offsets between the polymers and $PCBM$ (LUMO levels of -4.03 and -4.13 eV for $PC_{61}BM$ and PC_71BM , respectively),²⁵ which are considered to provide the driving force for exciton dissociation as well as to prevent recombination of photogenerated charges, are small (<0.2 eV) but may still be sufficient.^{10c}

Theoretical Calculations. Quantum-chemical calculations by the density functional theory (DFT) at the B3LYP/6-31G(d) level²⁶ using the Gaussian 09 program²⁷ were employed to demonstrate the electronic structure of these polymers. For computational simplification, the alkyl side chains on the isoindigo unit were replaced with methyl groups, the alkoxy side chains on the BDT unit were replaced with methoxy groups, and the branched alkyl side chains on the BDT were replaced with the equivalent ethyl side chains; and the backbones were simplified to two repeating units. For PMIM, which has the shortest conjugation path length, we also extended the computation to three repeating units. All of the optimized molecular structures are in a stable local minimum of the ground state potential energy surface, and analytical second derivatives of the Hessian matrix were calculated at the same level of theory to ensure this. The optimized molecular geometries of the models and their calculated frontier orbitals are depicted in Table S1 (Supporting Information). The dihedral angles are given in Table 1. Without insertion of additional donor units, PMIM gives the most twisted (ca. 50°) optimized molecular geometry as can be seen from Table S1. The other three polymers can have a more coplanar conformation than PMIM. The torsion angles between the flanking methylthiophene and inserted donor units are more or

Table 1. Dihedral Angles (deg) along the Conjugated Backbone for the Optimized Molecular Geometries Obtained by DFT Evaluated at the B3LYP/6-31G(d) Level

	D	$\theta_1(CCCC)^a$	$\theta_2(CCCC)^a$	$\theta_3(CCCC)^a$
PMIM	without	-	-	49.0
PT-MIM		21.4	21.7	37.7 (0.7) ^b
PBDTO-MIM		23.6	15.9	8.1
PBDTA-MIM		24.7	23.9	0.9

^aAll the values are given as positive angles from planarity with all the adjacent thiophenes adopting anti-conformations. ^bEvaluated with the terthiophene in a helical conformation, the value in the parentheses corresponding to a zigzag conformation.

Table 2. Photovoltaic Parameters, under Standard Illumination, of the BHJ PSCs and Corresponding Charge Mobilities

polymer:acceptor ratio (w/w)	solvent	thickness (nm)	DIO (% v/v)	annealing <i>T</i> ^a (°C)	<i>J</i> _{SC} (mA cm ⁻²)	<i>V</i> _{OC} (V)	FF (%)	PCE ^b (%)	(cm ² V ⁻¹ s ⁻¹)
PMIM:PC ₆ BM (1:1)	CHCl ₃	85	2	90	6.24	0.73	36	1.64 (1.5)	7.4 × 10 ⁻⁵
PT-MIM:PC ₆ BM (1:1)	CHCl ₃	110	1		10.41	0.71	43	3.14 (3.1)	1.0 × 10 ⁻⁴
PBDTO-MIM:PC ₆ BM (1:1.5)	CHCl ₃ :DCB (1:1)	130	3	110	10.09	0.73	59	4.36 (3.9)	1.5 × 10 ⁻⁴
PBDA-MIM:PC ₆ BM (1:1.5)	CHCl ₃ :DCB (1:1)	140	3		10.20	0.80	65	5.36 (5.1)	2.7 × 10 ⁻⁴
PMIM:PC ₇ BM (1:1)	CHCl ₃	85	2	90	6.54	0.71	33	1.54 (1.5)	6.0 × 10 ⁻⁵
PT-MIM:PC ₇ BM (1:1)	CHCl ₃	95	1		10.56	0.70	48	3.55 (3.4)	1.1 × 10 ⁻⁴
PBDTO-MIM:PC ₇ BM (1:1.5)	CHCl ₃ :DCB (1:1)	125	3	110	10.70	0.73	64	4.98 (4.9)	2.9 × 10 ⁻⁴
PBDA-MIM:PC ₇ BM (1:1.5)	CHCl ₃ :DCB (1:1)	135	3		9.47	0.80	61	4.60 (4.4)	1.2 × 10 ⁻⁴

^aAnnealing time: 10 min. ^bPower conversion efficiencies of the best devices, with average values based on over six devices given in parentheses.^cHole mobility estimated by space charge limited current (SCLC) method.

less the same, around 20°. For PT-MIM, it is also possible to give a flat angle of θ_3 similar to the BDT-based polymers, given the rigidity and symmetry of the inserted units. As the side chains on the flanking thiophene are very short (just methyl groups for the synthesized PT-MIM), they do not force the terthiophene units to adopt conformations that place the side chains away from each other.¹¹ The high planarity of the backbones in these three conjugation-extended polymeric systems, which was also shown for PBDT-TIT in our recent modeling work,²⁸ could favor the $\pi-\pi$ stacking interactions that occur among the polymer backbones in the solid state, which could in turn enhance the charge mobility (see mobility measurements in Table 2).¹¹

DFT showed very similar LUMOs for PMIM and PT-MIM, which are rather spatially delocalized, although the wave functions reside mainly on isoindigo units. Instead, for the BDT-based polymers, the LUMOs are more localized on the isoindigo units. The calculated LUMO levels (included in Figure 2) follow the order PBDTO-MIM (-2.87 eV) < PBDA-MIM (-2.85 eV) < PT-MIM (-2.83 eV) < PMIM (-2.81 eV). Both DFT and SWV showed that PBDTO-MIM has the lowest LUMO level. The other three polymers showed a slightly different order of LUMO levels evaluated by DFT calculations compared to the electrochemical measurements; however, the differences are very small (0.04 eV for DFT vs 0.03 eV for SWV). This also emphasizes that the LUMO level of the molecules is mainly governed by the acceptor units, with a small contribution from the donor units.²⁹ We also looked at the wave functions of the isolated donor units and found that the LUMOs of the resulting donor–acceptor molecules are the bonding linear combination from the LUMO of the isoindigo segment MIM with the respective LUMOs of the inserted donor units (Table S2). And the LUMO levels of the inserted donor units follow the order thiophene > BDTA > BDTO. As a consequence, the resulting LUMO levels followed the same order even though the difference is small as can be seen Figure 2, where PMIM has the highest LUMO level over the other three polymers evaluated by DFT based on the same number of repeating units. Similar phenomena were observed for the HOMOs of the polymers, but from the antibonding linear combination from the HOMOs of the corresponding separated segments (Table S2). Therefore, PMIM has the lowest HOMO level as confirmed by DFT, while the difference between the HOMOs of the other three polymers is even smaller. For all the

four polymers, the HOMOs are delocalized along the entire conjugated backbones (Table S1).

We also have to keep in mind the influence of different conjugation path lengths. By limiting the models to the same numbers of repeating units, systematic error cannot be avoided from such a low calculation level of oligomers. The conjugation path lengths in the calculations are quite often shorter than the effective conjugation lengths, and the change from incorporation of different donor units will definitely result in the variation in the conjugation path lengths. This will influence the extrapolation from the comparison of oligomers to that of polymers. For this reason, we also extended the DFT calculation for PMIM to three repeating units to have a similar conjugation path length to the BDT-based oligomers. The DFT-computed HOMO and LUMO energy levels are -5.06 and -2.86 eV, respectively. By increasing the number of repeating units from two to three, we see a ca. 0.05 eV decrease in the LUMO level and 0.02 eV in the HOMO level. Indeed, this will result in slightly different orders of the values, but we can further confirm that the LUMO levels are governed by the acceptor units and that PMIM has the lowest HOMO level and the largest LUMO–HOMO energy gap among the four isoindigo-based polymers in the gas phase.

We also have to mention that the removal of oxygen from the side chains normally results in a deeper HOMO level, but this was not observed by DFT for the two BDT-based polymers with the same conjugated backbone. This turns out to be accountable for the mismatch of the trends in HOMO levels from DFT in comparison with electrochemical measurements. On the other hand, given the fact that the DFT calculations are based on the gas phase while the experimental results are from solid states or solution, variations in the trend of the energy levels between experimental measurements and theoretical calculations may occur, but this may give a hint to extrapolate the results from DFT to understand the difference between different physical states.

Furthermore, we also performed single-point calculations at the B3LYP/6-31G(d) level of theory on the planar geometries which were derived from the corresponding optimized geometries at the same level of theory by forcing the dihedral angles along the conjugated backbones to be planar. The energy difference of the forced planar geometry and the optimized geometry is summarized in Table S3. This was done to gain more insights about how much energy may be required to planarize the polymer backbone in order to optimize solid

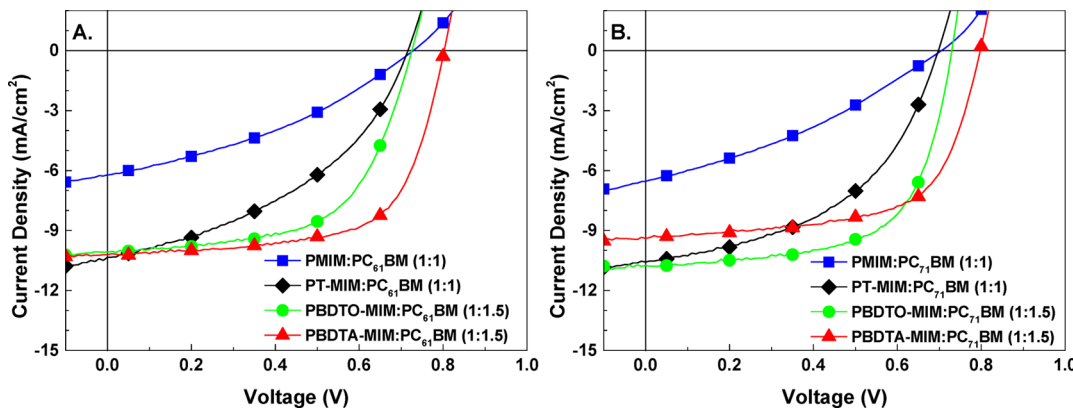


Figure 3. J – V curves of the optimized BHJ PSCs from the four isoindigo-based polymers with (A) PC_{61}BM and (B) PC_{71}BM as the acceptor.

state packing.¹¹ It has to be noted that solid state packing does not necessarily cause the polymer backbones to be totally planar, and therefore the backbone planarization energy calculated here can be regarded as the upper limit of the energy required to planarize the backbone upon solid state packing. Because the substitutions on the thiophenes are only methyl groups, it is possible to have a more planar backbone upon solid state packing for PMIM. It is found that due to the steric hindrance in the presence of head-to-head linkages between the adjacent substituted thiophene rings in the donor moiety, the backbone planarization energy for PMIM (10.2 kcal/mol for the two repeating unit and 19.3 kcal/mol for the three repeating unit) is much larger than the other three polymers (4.5, 4.0, and 4.8 kcal/mol for PT-MIM, PBDTO-MIM, and PBDTA-MIM, respectively, based on two repeating units), as can be seen from Table S3. Considering the temperature and energy gain upon stacking, it is reasonable that the planarization energies can be overcome. This will result in a possibility that in the solid state the LUMO–HOMO energy gaps of the four isoindigo-based polymers may follow the same trend as the optical gaps (increasing in the order of PMIM < PT-MIM < PBDTO-MIM ≈ PBDTA-MIM).

Time-dependent DFT (TD-DFT) calculations³⁰ were performed to assess the excited-state vertical transition energies and oscillator strengths based on the optimized molecular geometries at the same level of theory. We find that for all the polymers all the transitions in the visible region correspond to $\pi-\pi^*$ transitions. In particular, the lowest excitations are all dominated by the HOMO → LUMO transitions as can be seen from Figure S3 and Table S4.³¹ The higher energy excitation bands are also of $\pi-\pi^*$ character by checking the orbitals in the major contribution of transitions given in Table S4 and are primarily from local excitations. The BDT-based polymers show comparable lowest excitation energies, oscillator strengths, and high absorption coefficients, with the same conjugation path length. PT-MIM also showed comparable absorption properties to BDT-based polymers considering that PT-MIM in our calculation has a slightly shorter conjugation path length (22 double bonds for PT-MIM vs 26 for PBDTO-MIM and PBDTA-MIM). PMIM has the shortest conjugation path length in the two-repeating-unit models (18 double bonds), which may render a similar absorption pattern to the other polymers when computed with comparable conjugation path lengths. For this reason, we also performed TD-DFT for PMIM with three repeating units based on the optimized molecular geometry at the same level of theory (Table S4 and

Figure S3). We find that PMIM indeed has a comparable oscillator strength to the other three polymers and still the maximum lowest excitation energy, consistent with the largest DFT-derived LUMO–HOMO energy gap among the four polymers. This polymer, however, has the smallest optical gap among the four isoindigo-based polymers deduced from their film absorption edges. We therefore postulate that the extension of conjugation for PMIM going from the gas phase to the solid state may be due to a more coplanar conformation favored by intermolecular interactions.

We have further looked at the SWV measurements to understand the mismatch of the trend of the measured and calculated HOMO and LUMO levels. Energy levels deduced from the onsets of the first oxidation and reduction potentials were therefore included in Figure 2 for comparison. The trend of LUMO levels from these onsets is consistent with the calculated trend, which is PBDTO-MIM < PBDTA-MIM < PT-MIM ≈ PMIM. The measured HOMO levels and band gaps follow the trends from DFT calculations except for PBDTA-MIM due to the aforementioned reasons.

Photovoltaic Performance. In order to investigate the effect of incorporating different electron-rich thiophene-based units into the polymer backbones on the photovoltaic properties, BHJ PSCs based on the new donor polymers (D) combined with PC_{61}BM (or PC_{71}BM) as the acceptor (A) were fabricated using a conventional device configuration (glass/ITO/PEDOT:PSS/active layer/LiF/Al). Further details for the device fabrication and characterization are given in the experimental section. Table 2 and Table S5 summarize the photovoltaic responses of optimized devices. Representative current density–voltage (J – V) plots, measured under standard illumination (AM1.5G, 100 mW cm⁻²), are shown in Figure 3.

To better evaluate the structure–property relationships of the different isoindigo-based conjugated polymers, first PSC optimization was carried out by using PC_{61}BM as the acceptor material (Table 2, Table S5, and Figure 3A). The optimal D:A ratio (w/w) was found to be 1:1 for PMIM and PT-MIM or 1:1.5 for PBDTO-MIM and PBDTA-MIM. The slight difference could be ascribed to the different relative molecular masses, solubility, and interchain packing tendencies of the two series of polymers.³² Upon increasing or decreasing the D:A ratios of the active blends from their optimized values, a significant drop in J_{SC} , V_{OC} , or FF was observed, resulting in lower PCEs (Table S5).

Several efforts to optimize the thin-film nanomorphology of the polymer: PC_{61}BM devices were carried out (Table S5) using

different solvents (e.g., chloroform, chlorobenzene, or *o*-dichlobenzene) and thermal annealing (in the range 80–140 °C and for different times). Alternative approaches to enhance solar cell performance included the use of (i) 1,8-diiodooctane (DIO) as a processing solvent additive and (ii) PC₇₁BM as the acceptor.

From the device based on PMIM:PC₆₁BM (1:1) fabricated from chloroform solution, a PCE of 0.09% with $V_{OC} = 0.78$ V, $J_{SC} = 0.55$ mA/cm², and FF = 22% was first recorded (Table S5). Since DIO was shown to be an effective processing additive for improving the morphology of the active layer^{49,33} and thereby enhancing the photovoltaic performance of isoindigo-based polymers in our previous studies,^{8d,i} 2% (v/v) of DIO was added to the solution of the active material in order to further optimize the PV performance. As a result, the J_{SC} of the device was improved up to 3.48 mA/cm², resulting in a PCE of 0.59%. In combination with thermal annealing at 90 °C for 10 min the PCE of the PMIM:PC₆₁BM-based device was further improved up to 1.64%, with $V_{OC} = 0.73$ V, $J_{SC} = 6.24$ mA/cm², and FF = 36% (Table 2). Compared to PMIM, PT-MIM:PC₆₁BM-based solar cells, processed with DIO, exhibit an almost doubled PCE (3.14%) mainly due to an increased photocurrent ($J_{SC} = 10.41$ mA/cm²). This correlates well with the higher hole mobility (μ_h) measured for PT-MIM than that for PMIM (mobilities estimated by space charge limited current (SCLC), Table 2). However, the V_{OC} and the FF (0.71 V and 43%, respectively) still indicate some morphological limitations in the optimization of the performances of the PT-MIM:PC₆₁BM-based device. Additional thermal treatment (110 °C, 10 min, Table S5) mainly led to a drop in J_{SC} , thus resulting in a lower PCE.

For PBDTO-MIM and PBDTA-MIM a mixture of chloroform and ODCB (1:1 v/v) was used as solvent, since higher relative molecular masses could be obtained for these polymers, implying a higher solubility in chlorinated aromatic solvents. The best-performing BHJ solar cells were obtained again when processed with DIO as the solvent additive. Because of their similar molecular structure, with the exception for the branched side chains (alkoxy or alkyl) on the BDT unit, both PBDTO-MIM:PC₆₁BM- and PBDTA-MIM:PC₆₁BM-based PSCs exhibit high PCEs (4.36% and 5.36%, respectively). In particular, the devices afford similarly high J_{SC} (~10 mA/cm²), in agreement with the high charge mobilities of the two polymers (Table 2). On the other hand, the optimized PBDTO-MIM:PC₆₁BM solar cell showed a relatively lower V_{OC} (0.73 V vs 0.80 V) than the PBDTA-MIM-based one, in agreement with the different HOMO energy levels measured for the two polymers (Figure 2). Despite the slight difference in the FF of the two devices, it is worth noting that the high J_{SC} (and PCE) obtained for the two devices mainly suggest good charge transport properties of both photoactive materials, as a result of the high polymer charge mobility and an optimal D:A self-organization in the solid state (see also Morphological Studies section).

Unlike PBDTO-MIM, the best photovoltaic response of PBDTA-MIM:PC₆₁BM-based cell was obtained for as-cast films. Indeed, a thermal annealing (110 °C 10 min) of the film leads to a drop in J_{SC} and PCE (similar to the case of PT-MIM, Table S5), suggesting a slightly different self-aggregation tendency despite their structural similarity. It is worth noting that the PCEs for PBDTO-MIM and PBDTA-MIM together with our previously reported PBDT-TIT and PBDT-OIO^{8l} follow the order PBDT-OIO (1.26%) < PBDT-TIT (4.22%) < PBDTO-MIM (4.36%) < PBDTA-MIM (5.36%). This

indicates that the introduction of methyl groups on the flanking thiophenes is indeed a simple and effective alternative synthetic strategy without sacrificing the photovoltaic performance or suffering the synthetic difficulty for example to make PBDT-TIT.^{8l} This strategy also allows one to design and synthesize new isoindigo-based polymers that combine many other different donor moieties in order to further explore possibilities of improving the photovoltaic performance without having to stay with the low-yielding synthesis of the dibromide monomer (i.e., *N,N'*-disubstituted-6,6'-bis(5-bromo-2-yl)isoindigo). It is known that having a simple, high-yielding synthetic route that will reduce materials cost is of critical importance for the future mass production of PSCs.

The open-circuit voltages of optimized BHJ PSCs for the four polymers combined with PC₆₁BM (Table 2) track the progression V_{OC} (PT-MIM) < V_{OC} (PMIM) ≈ V_{OC} (PBDTO-MIM) < V_{OC} (PBDTA-MIM) rather than V_{OC} (PT-MIM) < V_{OC} (PBDTO-MIM) < V_{OC} (PMIM) < V_{OC} (PBDTA-MIM) as expected from $E(\text{LUMO}_A) - E(\text{HOMO}_D)$ theoretical considerations.^{6b,34} The larger loss in V_{OC} for PMIM, despite its low-lying HOMO level, could be ascribed to its poor D:A phase segregation (see AFM images, Figure 5) and low exciton dissociation and charge transport—all factors that are known to influence the V_{OC} ³⁵ PT-MIM-, PBDTO-MIM-, and PBDTA-MIM-based solar cells, in agreement with the electrochemically derived $E(\text{LUMO}_A) - E(\text{HOMO}_D)$ offset and in combination with good film-forming properties, show smaller losses in V_{OC} , achieving relatively high V_{OC} (up to 0.8 V).

Therefore, from this set of optimized BHJ devices (based on PC₆₁BM), some effects of the chemical modifications of the polymer structures on the corresponding photovoltaic properties have been evidenced. The insertion of the thiophene moiety into the backbone, going from PMIM to PT-MIM, resulted in a decreased V_{OC} due to the raised HOMO level, but an almost doubled PCE was achieved coupled with a greatly increased J_{SC} due to the increased hole mobility. In addition, the replacement of a thiophene ring with a BDT moiety increased the V_{OC} and FF without losses in J_{SC} , leading to an enhanced PCE. More importantly, when alkoxy side chains on the BDT unit were replaced with analogous alkyl chains, the V_{OC} was further improved due to the deepening in the HOMO level, and the FF was further improved as well probably thanks to a modified morphological D:A blend arrangement. As a result, PBDTA-MIM, blended with PC₆₁BM, stands out as the best-performing photoactive material among these polymers, with a V_{OC} of 0.80 V, J_{SC} of 10.20 mA/cm², FF of 65%, and a PCE of 5.36%. This together with the desirable low optical gaps, the favorable polymer miscibility with PC₆₁BM and high open-circuit voltages as well as high PCEs, demonstrates the potential of this class of polymers as suitable donor candidates for use in bottom subcells of efficient tandem devices.

A new set of BHJ PSCs were prepared, based on the four polymers, by simply replacing PC₆₁BM with PC₇₁BM as the acceptor (using the optimized processing conditions found for PC₆₁BM) in order to improve the photovoltaic performance by enhancing the blend film absorption in the spectral range between 350 and 550 nm for increased J_{SC} .³⁶ The resulting photovoltaic performances are reported in Table 2, Table S5, and Figure 3B. The J_{SC} 's of optimized devices based on PMIM, PT-MIM, or PBDTO-MIM combined with PC₇₁BM were slightly increased, while the V_{OC} 's were the same or slightly reduced. As a consequence, by replacing PC₆₁BM with PC₇₁BM, the PCE remained almost identical for PMIM while

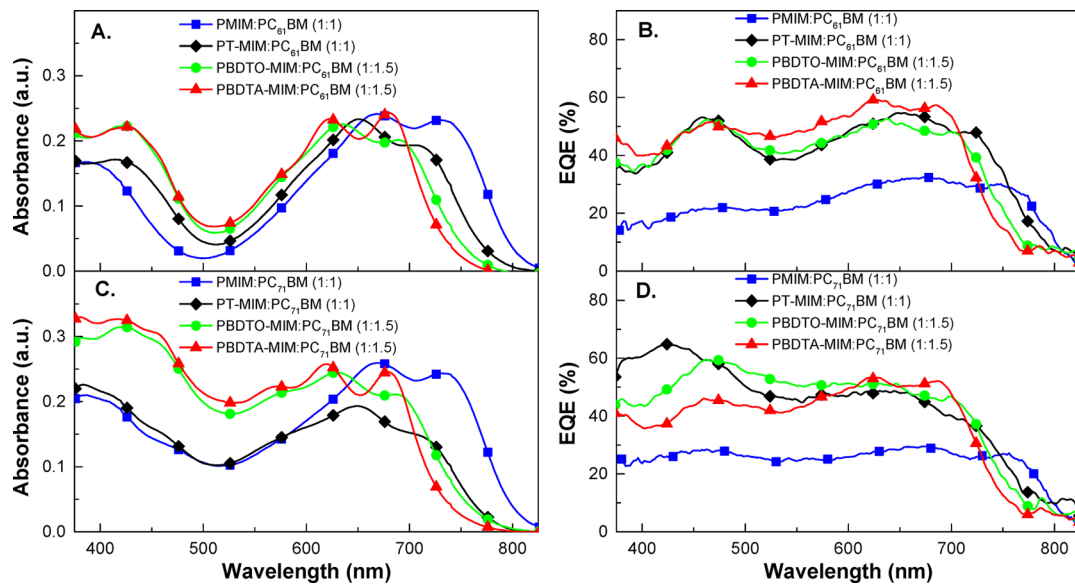


Figure 4. UV-vis absorption spectra and EQE plots of optimized BHJ solar cells.

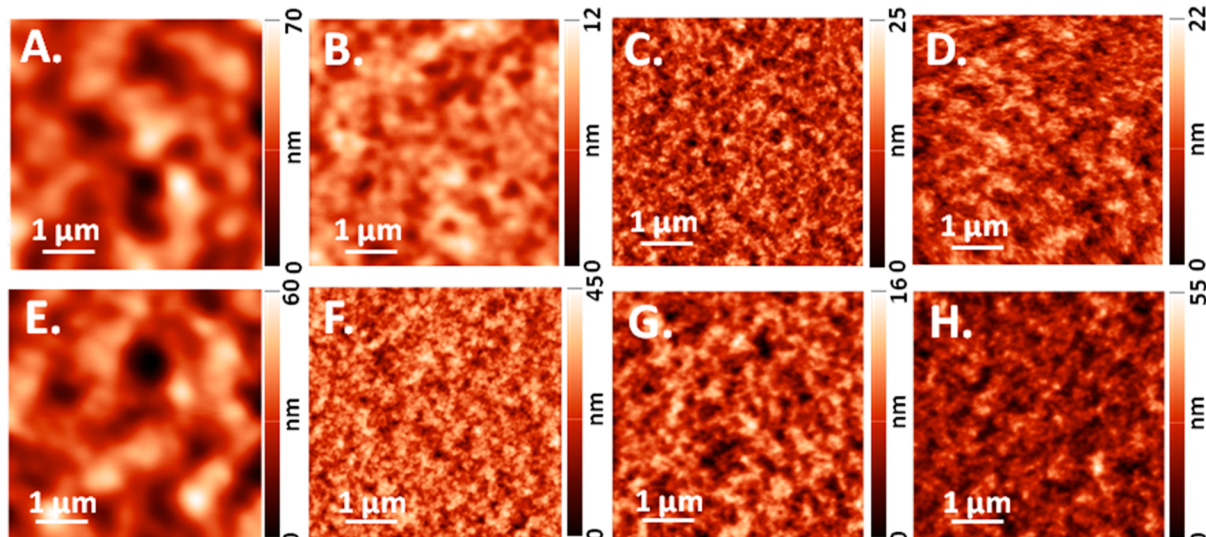


Figure 5. Tapping mode AFM images ($5 \mu\text{m} \times 5 \mu\text{m}$) of the active layers from the optimized BHJ PSCs based on (A) 1:1 (w/w) PMIM:PC₆₁BM (RMS = ~ 9.6 nm); (B) 1:1 (w/w) PT-MIM:PC₆₁BM (RMS = ~ 1.4 nm); (C) 1:1.5 (w/w) PBDTO-MIM:PC₆₁BM (RMS = ~ 3.2 nm); (D) 1:1.5 (w/w) PBDTA-MIM:PC₆₁BM (RMS = ~ 6.7 nm); (E) 1:1 (w/w) PMIM:PC₇₁BM (RMS = ~ 9.2 nm); (F) 1:1 (w/w) PT-MIM:PC₇₁BM (RMS = ~ 5.4 nm); (G) 1:1.5 (w/w) PBDTO-MIM:PC₇₁BM (RMS = ~ 2.3 nm); and (H) 1:1.5 (w/w) PBDTA-MIM:PC₇₁BM (RMS = ~ 6.1 nm).

for PT-MIM was increased from 3.14% to 3.55% and for PBDTO-MIM from 4.36% to 4.98%. PBDTA-MIM:PC₇₁BM-based cells exhibit, compared to the analogous PC₆₁BM-based devices, a slight drop in J_{SC} (from 10.20 to 9.47 mA/cm²) and FF (from 65% to 61%). This may suggest, in these conditions, a slightly poorer miscibility of PC₇₁BM with this polymer,^{49,36e} which partially hinders an optimal self-organization of the BHJ components, as also confirmed by the reduced hole mobility of PBDTA-MIM blended with PC₇₁BM (1.2×10^{-4} cm² V⁻¹ s⁻¹) compared to the analogous PC₆₁BM-based films (2.7×10^{-4} cm² V⁻¹ s⁻¹). In order to gain insight into these differences, deeper investigations and additional optimization processes are underway since higher PCEs can be reached, in particular using PBDTO-MIM and PBDTA-MIM as the donor and PC₇₁BM as the acceptor.

In order to enhance our understanding of the different photocurrent generation efficiencies, the spectral responses of

these devices were measured (Figure 4). The external quantum efficiency (EQE) spectra of the optimized BHJ PSCs with PC₆₁BM or PC₇₁BM as the acceptor (Figures 4B and 4D, respectively) are consistent with the broad optical absorption spectra of the active blends (Figures 4A and 4C, respectively). The EQE spectra for the optimized cells using PC₆₁BM as the acceptor (Figure 4B) exhibit the highest ratio of photo-generated electrons collected by the PSCs to incident photons in the spectral range between 590 and 710 nm, corresponding to the lower-energy absorption band of the polymers. Figure 4D shows the EQE responses of the most efficient PSCs using PC₇₁BM as the acceptor, in which the spectral profiles, compared to the corresponding PC₆₁BM-based devices, are mainly enhanced in the wavelength range between 380 and 530 nm, in agreement with the absorption profile of PC₇₁BM. As a consequence, the EQE in this spectral region showed maximum values of 30% (at 455 nm), 64% (at 430 nm), 59% (at 470 nm),

and 46% (at 460 nm) respectively for PMIM-, PT-MIM-, PBDTO-MIM-, and PBDTA-MIM-based PSCs with PC₇₁BM as the acceptor. Note that the red portion (>550 nm) of these EQE profiles is slightly reduced as a possible consequence of slightly different (induced) polymer self-organization or phase separation. Convolution of these EQE spectra with the AM1.5 solar spectrum gave calculated J_{SC} 's in good agreement, within a ~10% experimental error, with those obtained from $J-V$ measurements (Table S6).

Morphological Studies. It is known that the nanomorphology of the BHJ active layer plays an important role in determining the photovoltaic performance.^{35a,b,37} The morphological differences of the optimized polymer-based films were analyzed by tapping-mode atomic force microscopy (AFM). Figure 5 shows the topographic images of the films from the optimized PSCs (reported in Table 2) based on these polymers blended with either PC₆₁BM or PC₇₁BM.

The topographic image of PMIM:PC₆₁BM (Figure 5A) exhibits quite large and poorly defined domains, which may suggest a suboptimal phase segregation of the BHJ components. Thus, poorly formed percolation pathways lead to limited charge transport and/or collection processes within the active blends, as confirmed by the low EQE, J_{SC} , FF, PCE, and mobility obtained from the corresponding BHJ films. A similar nanomorphology can be observed also for the PT-MIM:PC₆₁BM-based film (Figure 5B), which correlates well with the low FF and charge mobility of the corresponding device. This could be ascribed to the relatively low molar masses and the relatively low D:A phase separation tendency of PMIM and PT-MIM. On the other hand, the slightly reduced domain sizes in PT-MIM:PC₆₁BM-based film compared to PMIM:PC₆₁BM-based one correlates well with the higher J_{SC} and hole mobility of the former one.

On the other hand, the surface morphologies of PBDTO-MIM:PC₆₁BM- and PBDTA-MIM:PC₆₁BM-based films (Figures 5C and 5D, respectively) are significantly different and characterized by reduced domain sizes with finer nanostructures, likely due to the presence of BDT units that favors a better intermolecular $\pi-\pi$ stacking and ordering of the polymer chains, which promotes a fine D:A intermixing with proper BHJ nanoscale phase separation, reflected in the higher photovoltaic performance of the resulting PBDTO-MIM- and PBDTA-MIM-based solar cells.

The AFM images of the analogous blends with PC₇₁BM (Figures 5E–H) reveal a nearly identical trend already observed for PC₆₁BM-based films without evident and/or significant variations, in agreement with the comparable electrical performance. Note that the PT-MIM:PC₇₁BM film (Figure 5F) exhibits more defined and structured domains which correlate well with the relatively increased FF and PCE. As mentioned above, the well-organized morphologies and the relatively high charge mobilities measured on PBDTO-MIM and PBDTA-MIM films confirm also in this case the formation of optimal nanoscale phase separation and interpenetrating networks in the entire photoactive layer, in agreement with the high FF and PCEs up to ~5% of these devices.

Finally, note that PBDTA-MIM-based films, independently from the acceptor material employed, exhibit well-organized and fine nanostructured motifs, highlighting an optimal self-organization and phase segregation tendency in BHJ layers, thus resulting in optimal electrical properties, with PCEs of ~5%, without the need of additional thermal treatments.

CONCLUSIONS

In summary, we have designed and synthesized four donor–acceptor conjugated alternating copolymers based on the same isoindigo acceptor unit, which combine different electron-rich thiophene-based donor moieties, in order to explore the potential of isoindigo-based polymers for efficient donor materials with high photovoltages in solar cells. We have systematically investigated the influence of the different electron-rich units on the structural, optical, electrochemical, and photovoltaic properties. Mobility measurements, morphological studies, and quantum-chemical calculations including DFT and TD-DFT were carried out to find out the insights into the differences. We find that the PCEs of the resulting PSCs can be improved by over 3-fold through a rational structural modification of the donor moiety, which highlights the importance of carefully choosing appropriate chemical structure to design efficient donor–acceptor polymers for solar cells. Among these polymers, PBDA-MIM exhibits a PCE of 5.4%, which is the highest value obtained for isoindigo-based polymers for conventional BHJ PSCs combined with PC₆₁BM as the acceptor to date. This further emphasizes the use of isoindigo as an effective acceptor unit for designing active donor materials and demonstrates the potential of this class of polymers as donor candidates for bottom cells in tandem devices, which combine low optical gaps, promising efficiencies, and desirable open-circuit voltages into isoindigo-based polymers with PC₆₁BM as the acceptor.

ASSOCIATED CONTENT

S Supporting Information

Experimental details, device fabrication and characterization, synthesis of monomers and polymers, square-wave voltammograms, additional data of DFT and TD-DFT calculations, details for optimizing processing conditions of solar cell fabrication and calculated short current densities for comparison of optimized cells, and abbreviations. This material is available free of charge via the Internet at <http://pubs.acs.org>.

AUTHOR INFORMATION

Corresponding Authors

*E-mail wenliu@chalmers.se (W.Z.).

*E-mail mats.andersson@chalmers.se (M.R.A.).

Notes

The authors declare no competing financial interest.

ACKNOWLEDGMENTS

This work was financially supported by the European Commission FP7 collaborative project SUNFLOWER (FP7-ICT-2011-7, Grant No. 287594). W.Z. also thanks the Swedish Energy Agency for financial support. We also acknowledge the Swedish Research Council and Chalmers' Area of Advance Materials Science for funding. The quantum chemical computations were performed on resources provided by the Swedish National Infrastructure for Computing (SNIC) at C³SE in Gothenburg. Anders Mårtensson was gratefully acknowledged for GPC characterizations and Timothy Steckler for fruitful discussions.

REFERENCES

- (a) Li, G.; Zhu, R.; Yang, Y. *Nat. Photonics* **2012**, *6*, 153–161.
- (b) Brabec, C. J. *Sol. Energy Mater. Sol. Cells* **2004**, *83*, 273–292.
- (c) Wang, E.; Wang, L.; Lan, L.; Luo, C.; Zhuang, W.; Peng, J.; Cao, Y.

- Appl. Phys. Lett.* **2008**, *92*, 033307. (d) Zhen, H. Y.; Li, K.; Huang, Z. Y.; Tang, Z.; Wu, R. M.; Li, G. L.; Liu, X.; Zhang, F. L. *Appl. Phys. Lett.* **2012**, *100*, 213901. (e) Bolognesi, M.; Tessarolo, M.; Posati, T.; Nocchetti, M.; Benfenati, V.; Seri, M.; Ruani, G.; Muccini, M. *Org. Photon. Photovolt.* **2013**, *1*, 1–10.
- (2) Yu, G.; Gao, J.; Hummelen, J. C.; Wudl, F.; Heeger, A. J. *Science* **1995**, *270*, 1789–1791.
- (3) (a) Service, R. F. *Science* **2011**, *332*, 293. (b) He, Z. C.; Zhong, C. M.; Su, S. J.; Xu, M.; Wu, H. B.; Cao, Y. *Nat. Photonics* **2012**, *6*, 591–595. (c) Small, C. E.; Chen, S.; Subbiah, J.; Amb, C. M.; Tsang, S.-W.; Lai, T.-H.; Reynolds, J. R.; So, F. *Nat. Photonics* **2011**, *6*, 115–120. (d) McCulloch, I. *Adv. Mater.* **2013**, *25*, 1811–1812.
- (4) (a) Chen, H. Y.; Hou, J. H.; Zhang, S. Q.; Liang, Y. Y.; Yang, G. W.; Yang, Y.; Yu, L. P.; Wu, Y.; Li, G. *Nat. Photonics* **2009**, *3*, 649–653. (b) Liang, Y. Y.; Feng, D. Q.; Wu, Y.; Tsai, S. T.; Li, G.; Ray, C.; Yu, L. P. *J. Am. Chem. Soc.* **2009**, *131*, 7792–7799. (c) Liang, Y. Y.; Xu, Z.; Xia, J. B.; Tsai, S. T.; Wu, Y.; Li, G.; Ray, C.; Yu, L. P. *Adv. Mater.* **2010**, *22*, E135–E138. (d) Huo, L.; Zhang, S.; Guo, X.; Xu, F.; Li, Y.; Hou, J. *Angew. Chem., Int. Ed.* **2011**, *50*, 9697–9702. (e) Zhou, H. X.; Yang, L. Q.; Stuart, A. C.; Price, S. C.; Liu, S. B.; You, W. *Angew. Chem., Int. Ed.* **2011**, *50*, 2995–2998. (f) Price, S. C.; Stuart, A. C.; Yang, L.; Zhou, H.; You, W. *J. Am. Chem. Soc.* **2011**, *133*, 4625–4631. (g) Huang, Y.; Guo, X.; Liu, F.; Huo, L.; Chen, Y.; Russell, T. P.; Han, C. C.; Li, Y.; Hou, J. *Adv. Mater.* **2012**, *24*, 3383–3389. (h) Piliego, C.; Holcombe, T. W.; Douglas, J. D.; Woo, C. H.; Beaujuge, P. M.; Frechet, J. M. J. *J. Am. Chem. Soc.* **2010**, *132*, 7595–7597. (i) Chu, T.-Y.; Lu, J.; Beaupré, S.; Zhang, Y.; Pouliot, J.-R.; Wakim, S.; Zhou, J.; Leclerc, M.; Li, Z.; Ding, J.; Tao, Y. *J. Am. Chem. Soc.* **2011**, *133*, 4250–4253. (j) Amb, C. M.; Chen, S.; Graham, K. R.; Subbiah, J.; Small, C. E.; So, F.; Reynolds, J. R. *J. Am. Chem. Soc.* **2011**, *133*, 10062–10065. (k) Chen, H.-C.; Chen, Y.-H.; Liu, C.-C.; Chien, Y.-C.; Chou, S.-W.; Chou, P.-T. *Chem. Mater.* **2012**, *24*, 4766–4772. (l) Chang, C. Y.; Cheng, Y. J.; Hung, S. H.; Wu, J. S.; Kao, W. S.; Lee, C. H.; Hsu, C. S. *Adv. Mater.* **2012**, *24*, 549–553. (m) Xu, Y.-X.; Chueh, C.-C.; Yip, H.-L.; Ding, F.-Z.; Li, Y.-X.; Li, C.-Z.; Li, X.; Chen, W.-C.; Jen, A. K. Y. *Adv. Mater.* **2012**, *24*, 6356–6361. (n) Guo, X.; Zhang, M.; Tan, J.; Zhang, S.; Huo, L.; Hu, W.; Li, Y.; Hou, J. *Adv. Mater.* **2012**, *24*, 6536–6541. (o) Son, H. J.; Lu, L.; Chen, W.; Xu, T.; Zheng, T.; Carsten, B.; Strzalka, J.; Darling, S. B.; Chen, L. X.; Yu, L. *Adv. Mater.* **2012**, *25*, 838–843. (p) Dou, L.; Chang, W.-H.; Gao, J.; Chen, C.-C.; You, J.; Yang, Y. *Adv. Mater.* **2012**, *25*, 825–831. (q) Su, M. S.; Kuo, C. Y.; Yuan, M. C.; Jeng, U. S.; Su, C. J.; Wei, K. H. *Adv. Mater.* **2011**, *23*, 3315–3319.
- (5) Havinga, E. E.; ten Hoeve, W.; Wynberg, H. *Polym. Bull.* **1992**, *29*, 119–126.
- (6) (a) Roncali, J. *Chem. Rev.* **1997**, *97*, 173–206. (b) Scharber, M. C.; Wuhlbacher, D.; Koppe, M.; Denk, P.; Waldauf, C.; Heeger, A. J.; Brabec, C. L. *Adv. Mater.* **2006**, *18*, 789–794. (c) Bredas, J. L.; Norton, J. E.; Cornil, J.; Coropceanu, V. *Acc. Chem. Res.* **2009**, *42*, 1691–1699. (d) Zhou, H. X.; Yang, L. Q.; Stoneking, S.; You, W. *ACS Appl. Mater. Interfaces* **2010**, *2*, 1377–1383. (e) Zhou, H.; Yang, L.; You, W. *Macromolecules* **2012**, *45*, 607–632.
- (7) (a) Dennler, G.; Scharber, M. C.; Brabec, C. J. *Adv. Mater.* **2009**, *21*, 1323–1338. (b) Dennler, G.; Scharber, M. C.; Ameri, T.; Denk, P.; Forberich, K.; Waldauf, C.; Brabec, C. J. *Adv. Mater.* **2008**, *20*, 579–583.
- (8) (a) Mei, J. G.; Graham, K. R.; Stalder, R.; Reynolds, J. R. *Org. Lett.* **2010**, *12*, 660–663. (b) Stalder, R.; Mei, J.; Reynolds, J. R. *Macromolecules* **2010**, *43*, 8348–8352. (c) Zhang, G.; Fu, Y.; Xie, Z.; Zhang, Q. *Macromolecules* **2011**, *44*, 1414–1420. (d) Wang, E. G.; Ma, Z. F.; Zhang, Z.; Henriksson, P.; Inganäs, O.; Zhang, F. L.; Andersson, M. R. *Chem. Commun.* **2011**, *47*, 4908–4910. (e) Liu, B.; Zou, Y. P.; Peng, B.; Zhao, B.; Huang, K. L.; He, Y. H.; Pan, C. Y. *Polym. Chem.* **2011**, *2*, 1156–1162. (f) Graham, K.; Mei, J.; Stalder, R.; Shim, J.; Cheun, H.; So, F.; Steffy, F.; Kippelen, B.; Reynolds, J. R. *ACS Appl. Mater. Interfaces* **2011**, *3*, 1210–1215. (g) Lei, T.; Cao, Y.; Fan, Y.; Liu, C.-J.; Yuan, S.-C.; Pei, J. *J. Am. Chem. Soc.* **2011**, *133*, 6099–6101. (h) Stalder, R.; Mei, J.; Subbiah, J.; Grand, C.; Estrada, L. A.; So, F.; Reynolds, J. R. *Macromolecules* **2011**, *44*, 6303–6310. (i) Wang, E. G.; Ma, Z. F.; Zhang, Z.; Vandewal, K.; Henriksson, P.; Inganäs, O.; Zhang, F. L.; Andersson, M. R. *J. Am. Chem. Soc.* **2011**, *133*, 14244–14247. (j) Ma, Z. F.; Wang, E. G.; Vandewal, K.; Andersson, M. R.; Zhang, F. L. *Appl. Phys. Lett.* **2011**, *99*, 143302. (k) Mei, J.; Kim, D. H.; Ayzner, A. L.; Toney, M. F.; Bao, Z. *J. Am. Chem. Soc.* **2011**, *133*, 20130–20133. (l) Ma, Z. F.; Wang, E. G.; Jarvid, M. E.; Henriksson, P.; Inganäs, O.; Zhang, F. L.; Andersson, M. R. *J. Mater. Chem.* **2012**, *22*, 2306–2314.
- (9) Wahl, A.; Bagard, P. *Bull. Soc. Chim. Fr.* **1910**, *5*, 1039–1043.
- (10) (a) Hu, C.; Fu, Y.; Li, S.; Xie, Z.; Zhang, Q. *Polym. Chem.* **2012**, *3*, 2949–2955. (b) Stalder, R.; Grand, C.; Subbiah, J.; So, F.; Reynolds, J. R. *Polym. Chem.* **2012**, *3*, 89–92. (c) Vandewal, K.; Ma, Z. F.; Bergqvist, J.; Tang, Z.; Wang, E. G.; Henriksson, P.; Tvingstedt, K.; Andersson, M. R.; Zhang, F. L.; Inganäs, O. *Adv. Funct. Mater.* **2012**, *22*, 3480–3490. (d) Cao, K.; Wu, Z.; Li, S.; Sun, B.; Zhang, G.; Zhang, Q. *J. Polym. Sci., Part A: Polym. Chem.* **2013**, *51*, 94–100. (e) Xu, X. F.; Cai, P.; Lu, Y.; Choon, N. S.; Chen, J. W.; Hu, X.; Ong, B. S. *J. Polym. Sci., Part A: Polym. Chem.* **2012**, *51*, 424–434.
- (11) Ko, S.; Hoke, E. T.; Pandey, L.; Hong, S.; Mondal, R.; Risko, C.; Yi, Y.; Noriega, R.; McGehee, M. D.; Brédas, J.-L.; Salleo, A.; Bao, Z. *J. Am. Chem. Soc.* **2012**, *134*, 5222–5232.
- (12) Aleman, C.; Julia, L. *J. Phys. Chem.* **1996**, *100*, 1524–1529.
- (13) (a) Barbarella, G.; Zambianchi, M.; Bongini, A.; Antolini, L. *Adv. Mater.* **1992**, *4*, 282–285. (b) Fichou, D. *J. Mater. Chem.* **2000**, *10*, 571–588.
- (14) (a) Hou, J. H.; Chen, H. Y.; Zhang, S. Q.; Chen, R. I.; Yang, Y.; Wu, Y.; Li, G. *J. Am. Chem. Soc.* **2009**, *131*, 15586–15587. (b) Li, Z.; Lu, J. P.; Tse, S. C.; Zhou, J. Y.; Du, X. M.; Tao, Y.; Ding, J. F. *J. Mater. Chem.* **2011**, *21*, 3226–3233. (c) Shi, C. J.; Yao, Y.; Yang, Y.; Pei, Q. B. *J. Am. Chem. Soc.* **2006**, *128*, 8980–8986.
- (15) (a) Quillinan, A. J.; Khan, E. A.; Scheinmann, F. *J. Chem. Soc., Chem. Commun.* **1974**, 1030–1031. (b) Kobayashi, Y.; Murugesh, M. G.; Nakano, M.; Takahisa, E.; Usmani, S. B.; Ainai, T. *J. Org. Chem.* **2002**, *67*, 7110–7123. (c) Slocum, D. W.; Gierer, P. L. *J. Org. Chem.* **1976**, *41*, 3668–3673. (d) Beimling, P.; Koßmehl, G. *Chem. Ber.* **1986**, *119*, 3198–3203. (e) Anthony, J. E.; Brooks, J. S.; Eaton, D. L.; Parkin, S. R. *J. Am. Chem. Soc.* **2001**, *123*, 9482–9483.
- (16) (a) Xiang, N.; Huang, X.; Feng, X.; Liu, Y.; Zhao, B.; Deng, L.; Shen, P.; Fei, J.; Tan, S. *Dyes Pigm.* **2011**, *88*, 75–83. (b) Cai, T. Q.; Zhou, Y.; Wang, E. G.; Hellström, S.; Zhang, F. L.; Xu, S. A.; Inganäs, O.; Andersson, M. R. *Sol. Energy Mater. Sol. Cells* **2010**, *94*, 1275–1281.
- (17) Smith, K.; Barratt, M. L. *J. Org. Chem.* **2007**, *72*, 1031–1034.
- (18) Bao, Z. N.; Chan, W. K.; Yu, L. P. *J. Am. Chem. Soc.* **1995**, *117*, 12426–12435.
- (19) Lei, T.; Cao, Y.; Zhou, X.; Peng, Y.; Bian, J.; Pei, J. *Chem. Mater.* **2012**, *24*, 1762–1770.
- (20) Wegner, G. *Thin Solid Films* **1992**, *216*, 105–116.
- (21) Müller, C.; Wang, E.; Andersson, L. M.; Tvingstedt, K.; Zhou, Y.; Andersson, M. R.; Inganäs, O. *Adv. Funct. Mater.* **2010**, *20*, 2124–2131.
- (22) Risko, C.; McGehee, M. D.; Bredas, J. L. *Chem. Sci.* **2011**, *2*, 1200–1218.
- (23) (a) Yuan, M.-C.; Chiu, M.-Y.; Chiang, C.-M.; Wei, K.-H. *Macromolecules* **2010**, *43*, 6270–6277. (b) Guo, X.; Zhang, M. J.; Huo, L. J.; Xu, F.; Wu, Y.; Hou, J. H. *J. Mater. Chem.* **2012**, *22*, 21024–21031. (c) Peet, J.; Kim, J. Y.; Coates, N. E.; Ma, W. L.; Moses, D.; Heeger, A. J.; Bazan, G. C. *Nat. Mater.* **2007**, *6*, 497–500. (d) Muhlbaier, D.; Scharber, M.; Morana, M.; Zhu, Z. G.; Waller, D.; Gaudiana, R.; Brabec, C. *Adv. Mater.* **2006**, *18*, 2884.
- (24) Lei, T.; Dou, J.-H.; Pei, J. *Adv. Mater.* **2012**, *24*, 6457–6461.
- (25) (a) Wang, E.; Hou, L.; Wang, Z.; Hellström, S.; Mammo, W.; Zhang, F.; Inganäs, O.; Andersson, M. R. *Org. Lett.* **2010**, *12*, 4470–4473. (b) Wang, E.; Hou, L.; Wang, Z.; Ma, Z.; Hellström, S.; Zhuang, W.; Zhang, F.; Inganäs, O.; Andersson, M. R. *Macromolecules* **2011**, *44*, 2067–2073.
- (26) (a) Lee, C. T.; Yang, W. T.; Parr, R. G. *Phys. Rev. B* **1988**, *37*, 785–789. (b) Becke, A. D. *J. Chem. Phys.* **1993**, *98*, 5648–5652. (c) Hehre, W. J.; Ditchfield, R.; Pople, J. A. *J. Chem. Phys.* **1972**, *56*,

2257–2261. (d) Harihara, P. C.; Pople, J. A. *Theor. Chim. Acta* **1973**, *28*, 213–222.

(27) Frisch, M. J.; Trucks, G. W.; Schlegel, H. B.; Scuseria, G. E.; Robb, M. A.; Cheeseman, J. R.; Scalmani, G.; Barone, V.; Mennucci, B.; Petersson, G. A.; Nakatsuji, H.; Caricato, M.; Li, X.; Hratchian, H. P.; Izmaylov, A. F.; Bloino, J.; Zheng, G.; Sonnenberg, J. L.; Hada, M.; Ehara, M.; Toyota, K.; Fukuda, R.; Hasegawa, J.; Ishida, M.; Nakajima, T.; Honda, Y.; Kitao, O.; Nakai, H.; Vreven, T.; Montgomery, J. A., Jr.; Peralta, J. E.; Ogliaro, F.; Bearpark, M.; Heyd, J. J.; Brothers, E.; Kudin, K. N.; Staroverov, V. N.; Keith, T.; Kobayashi, R.; Normand, J.; Raghavachari, K.; Rendell, A.; Burant, J. C.; Iyengar, S. S.; Tomasi, J.; Cossi, M.; Rega, N.; Millam, J. M.; Klene, M.; Knox, J. E.; Cross, J. B.; Bakken, V.; Adamo, C.; Jaramillo, J.; Gomperts, R.; Stratmann, R. E.; Yazyev, O.; Austin, A. J.; Cammi, R.; Pomelli, C.; Ochterski, J. W.; Martin, R. L.; Morokuma, K.; Zakrzewski, V. G.; Voth, G. A.; Salvador, P.; Dannenberg, J. J.; Dapprich, S.; Daniels, A. D.; Farkas, O.; Foresman, J. B.; Ortiz, J. V.; Cioslowski, J.; Fox, D. J. *Gaussian 09, Revision B.01*; Gaussian, Inc.: Wallingford, CT, 2010.

(28) Salvatori, P.; Mosconi, E.; Wang, E.; Andersson, M. R.; Muccini, M.; De Angelis, F. *J. Phys. Chem. C* **2013**, *117*, 17940–17954.

(29) Chang, H.-H.; Tsai, C.-E.; Lai, Y.-Y.; Chiou, D.-Y.; Hsu, S.-L.; Hsu, C.-S.; Cheng, Y.-J. *Macromolecules* **2012**, *45*, 9282–9291.

(30) Casida, M. E. *J. Mol. Struct.: THEOCHEM* **2009**, *914*, 3–18.

(31) O'Boyle, N. M.; Tenderholt, A. L.; Langner, K. M. *J. Comput. Chem.* **2008**, *29*, 839–845.

(32) Brabec, C. J.; Dyakonov, V.; Parisi, J.; Sariciftci, N. S. *Organic Photovoltaics: Concepts and Realization*; Springer-Verlag: Berlin, 2003; Vol. 60.

(33) (a) Lee, J. K.; Ma, W. L.; Brabec, C. J.; Yuen, J.; Moon, J. S.; Kim, J. Y.; Lee, K.; Bazan, G. C.; Heeger, A. J. *J. Am. Chem. Soc.* **2008**, *130*, 3619–3623. (b) Liu, X. L.; Huettner, S.; Rong, Z. X.; Sommer, M.; Friend, R. H. *Adv. Mater.* **2012**, *24*, 669–674. (c) Rogers, J. T.; Schmidt, K.; Toney, M. F.; Kramer, E. J.; Bazan, G. C. *Adv. Mater.* **2011**, *23*, 2284–2288.

(34) Brabec, C. J.; Cravino, A.; Meissner, D.; Sariciftci, N. S.; Fromherz, T.; Risپens, M. T.; Sanchez, L.; Hummelen, J. C. *Adv. Funct. Mater.* **2001**, *11*, 374–380.

(35) (a) Perez, M. D.; Borek, C.; Forrest, S. R.; Thompson, M. E. *J. Am. Chem. Soc.* **2009**, *131*, 9281–9286. (b) Stevens, D. M.; Speros, J. C.; Hillmyer, M. A.; Frisbie, C. D. *J. Phys. Chem. C* **2011**, *115*, 20806–20816. (c) Liu, J.; Shi, Y. J.; Yang, Y. *Adv. Funct. Mater.* **2001**, *11*, 420–424.

(36) (a) Wienk, M. M.; Kroon, J. M.; Verhees, W. J. H.; Knol, J.; Hummelen, J. C.; van Hal, P. A.; Janssen, R. A. J. *Angew. Chem., Int. Ed.* **2003**, *42*, 3371–3375. (b) Morana, M.; Wegscheider, M.; Bonanni, A.; Kopidakis, N.; Shaheen, S.; Scharber, M.; Zhu, Z.; Waller, D.; Gaudiana, R.; Brabec, C. *Adv. Funct. Mater.* **2008**, *18*, 1757–1766. (c) Sariciftci, N. S.; Smilowitz, L.; Heeger, A. J.; Wudl, F. *Science* **1992**, *258*, 1474–1476. (d) Hummelen, J. C.; Knight, B. W.; LePeq, F.; Wudl, F.; Yao, J.; Wilkins, C. L. *J. Org. Chem.* **1995**, *60*, 532–538. (e) Zhang, F.; Zhuo, Z.; Zhang, J.; Wang, X.; Xu, X.; Wang, Z.; Xin, Y.; Wang, J.; Wang, J.; Tang, W.; Xu, Z.; Wang, Y. *Sol. Energy Mater. Sol. Cells* **2012**, *97*, 71–77.

(37) (a) Dang, M. T.; Hirsch, L.; Wantz, G.; Wuest, J. D. *Chem. Rev.* **2013**, *113*, 3734–3765. (b) Moule, A. J.; Meerholz, K. *Adv. Funct. Mater.* **2009**, *19*, 3028–3036.